Morphology-Controlled Preparation of Heteropolyanion-Derived Mesoporous Solid Base

Xiaochen Wang, Yu Zhou, Guojian Chen, Jing Li, Zhouyang Long, and Jun Wang*

State Key Laboratory of Materials-Oriented Chemical Engineering, College of Chemistry and Chemical Engineering, Nanjing Tech University, Nanjing 210009, China

S *Supporting Information*

ABSTRACT: Heteropolyanion-derived mesoporous solid base catalysts were prepared by designing the basic ionic liquid (IL) N-3-[2-(2-aminoethylamino)ethylamino]-2-hydroxypropyl)-pyridinium chloride ([TAHpy]Cl) to assemble with Keggin-structured sodium phosphotungstate ($Na_3PW_{12}O_{40}$) in the aqueous solution containing organic base diethylenetriamine (DETA). The obtained hybrids were characterized by various techniques such as thermogravimetric analysis, elemental analysis, Fourier transform infrared spectroscopy, scanning electron microscope, and nitrogen adsorption experiments. In the synthesis, the concentration of DETA was adjusted to control the morphology and mesostructure of the obtained basic hybrids, and concentrated DETA caused the formation of the mesoporous solid base. The structure analysis indicated that the obtained hybrid demonstrated a piece-like shape in macroscopical size, and these species were assembled by relative uniform small nanoellipsoids with the diameter of ∼50 nm, which forms a loosely packed structure. Assessed in the liquid−solid heterogeneous Knoevenagel condensation, the mesoporous solid base with a morphology of loosely packed nanoparticles presented superior activity, which was about 14 times higher than the nonporous analogues with large block morphology. A possible catalytic mechanism is proposed to explain the efficient catalytic performance.

KEYWORDS: *Heterogeneous catalyst, Morphology and pore control, Mesoporous solid base, Polyoxometalate, Ionic liquids*
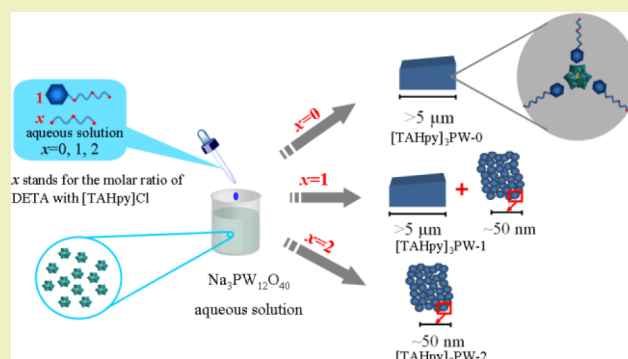
■ INTRODUCTION

Heterogeneous catalysis is one prominent technology for sustainable developments because it promotes the separation and reusability of the catalysts and ultimately benefits energy saving and environmental friendly processes.[1−3] However, heterogeneous catalysts usually suffer from inferior catalytic performance, and the major limitation arises because the accessibility of the active sites in heterogeneous catalysis is hard to compare to the homogeneous counterpart.[4] To overcome the above drawback, many researches focus on the morphology and pore structure control of the heterogeneous catalysts, in which an ideal situation is to assemble the active site-involved nanobuilding blocks into well-defined sizes and shapes with suitable porous frameworks.[5−7]

Polyoxometalates (POMs) have achieved diverse applications in chemistry-connected research fields such as catalysis, material science, medicine, etc. because their chemical and physical properties can be finely tuned by choosing constituent elements and countercations.[8] Therefore, POMs are suitable nanobuilding blocks for constructing functional materials through controlled self-assembly.[9−12] Many efforts have been made to the assembly of POM-anions, especially hetero-polyanion (HPA), for preparing efficient heterogeneous catalysts for numerous organic reactions.[13,14] However, the

major applications of these HPA-based catalysts focus on oxidation and acid-catalyzed reactions that rarely relate to base-catalyzed reactions. To date, only highly negative or charge density-enriched HPAs have been reported as homogeneous basic catalysts,[15−17] and no HPA-derived mesoporous solid base has appeared to the best of our knowledge, possibly due to the extreme difficulty in creating basic sites on mesoporous heterogeneous HPA-derived catalysts.

Among various modifiers for POMs,[18−20] ionic liquids (ILs) have been used as adjustable organic blocks that can be ionically linked with POM-anions. As is known, ILs are novel solvents/catalysts for organic transformations and materials syntheses, taking advantage of their negligible volatility, good thermal stability, and flexible structural designability.[21−23] In particular, "task-specific" basic IL catalysts with high activity and selectivity have been prepared by tethering basic functional groups onto IL-cations, which are regarded as alternatives other than traditional bases.[24,25] For example, the basic IL 1-butyl-3-methylimidazolium hydroxide ([bmIm]OH) has been used as both catalyst and reaction medium for Michael addition.[26] 1-

Butyl-4-aza-1-azoniabicyclo[2.2.2]-octane tetrafluoroborate was revealed to be an effective basic IL catalyst for Knoevenagel condensation.[27] When IL-cations were used as modifiers for HPAs, the obtained HPA salts with IL-like structures were mostly in solid state due to the high valence and large volume of HPAs.[28,29] As a result, the prepared IL-HPA hybrids mostly act as heterogeneous catalysts for organic syntheses, and in this context, through designing functional IL-cations, more and more IL-HPA catalysts appeared for acid-catalyzed reactions,[30−32] as well as oxidation processes.[33−35] In heterogeneous catalysis, catalyst morphology and pore structure determine the accessibility and exposure of the active sites, which strongly influence the mass transfer in reaction and thus the catalytic efficiency. However, the already-obtained IL-HPA hybrids usually show solidified morphology and pore structure, which arises from the difficulty in controlling morphology and porosity due to rapid assembly between IL-cations and HPA in catalyst preparation.

Herein, we specifically design a basic IL N-(3-[2-(2-amino-ethylamino)ethylamino]-2-hydroxypropyl)pyridineium chloride ([TAHpy]Cl) and combine it with Keggin-structured HPA $PW_{12}O_{40}{}^{3-}$ (PW) for preparing a heteropolyanion-derived mesoporous solid base catalyst through self-assembly (Scheme 1). During the process, additional diethylenetriamine (DETA)

Scheme 1. Synthetic Route to IL-HPA Hybrids [TAHpy]₃PW-x
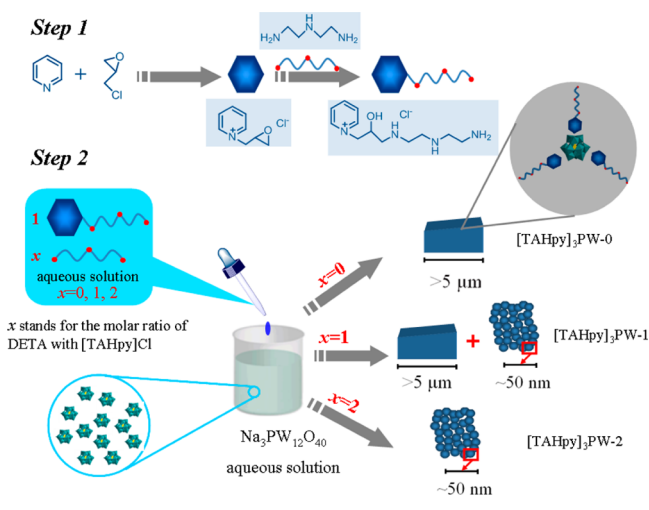
is introduced into the synthetic solution to control the morphology and porous structure during the self-assembly process of the IL-HPA. The catalytic performance of the obtained solid base is evaluated in Knoevenagel condensation of benzaldehyde with ethyl cyanoacetate, a typical model reaction for evaluating a basic catalyst. Various counterpart hybrids are also synthesized (Scheme S1, Supporting Information) to understand the morphology, pore structure control process, and catalytic activity.

■ EXPERIMENTAL SECTION

Materials and Methods. All the chemicals were of analytical grade and used as received. FT-IR spectra were recorded on a Nicolet iS10 FT-IR instrument (KBr disks) in the region of 4000−400 cm⁻¹. ¹H NMR spectra and ¹³C NMR spectra were measured with a Bruker DPX 500 spectrometer at ambient temperature by using D₂O as the solvent and TMS (tetramethylsilane) as internal reference. Elemental analyses were performed on a CHN elemental analyzer Vario EL cube.

XRD patterns were collected on a Smart Lab diffractmeter from Rigaku equipped with a 9 kW rotating anode Cu source at 45 kV and 200 mA from 5° to 50° with a scan rate of 0.2° s⁻¹. SEM images were obtained on a Hitachi S-4800 field-emission scanning electron microscope. BET surface areas were measured at the temperature of liquid nitrogen (77 K) by using a BELSORP-MINI analyzer, and the samples were degassed at 150 °C for 3 h before analysis. TG analysis was performed with an STA 409 instrument in dry air at a heating rate of 10 °C min⁻¹. Solid UV−vis spectra were measured with a SHIMADZU UV-260 spectrometer, and BaSO₄ was used as an internal standard.

Catalyst Preparation. Scheme 1 displayed the two-step process of the catalysts. N-Glycidylpyridinium chloride ([GIpy]Cl) was synthesized according to the literature.[36] ¹H NMR (300 MHz, D₂O, TMS) δ (ppm): 8.97−8.91 (m, 2H, ring), 8.72−8.67 (m, 1H, ring), 8.22−8.17 (m, 2H, ring), 5.11−4.68 (m, 1H, CHOCH₂), 3.85−3.84 (m, 2H, CHOCH₂), 1.2−1.17 (d, 2H, CH₂−N_ring). N-(3-[2-(2-Aminoethylamino)ethylamino]-2-hydroxypropyl)pyridinium chloride ([TAHpy]Cl) was prepared by a ring-opening reaction between [GIpy]Cl and diethylenetriamine (DETA). Methanol (solvent, 15 mL), [GIpy]Cl (1 g, 6 mmol), and DETA (1.25 g, 12 mmol) were mixed in a flask and stirred under refluxing at 70 °C for 24 h. After the reaction, solvent was removed by rotary evaporation, and the crude product was dried under vacuum for 12 h. The product was purified through recrystallization from the dry cold acetone, giving a brown solid (Yield: 45%). ¹H NMR (300 MHz, D₂O, TMS) δ (ppm): 8.95−8.87 (m, 2H, ring), 8.69−8.64 (m, 1H, ring), 8.19−8.14 (m, 2H, ring), 5.11−4.68 (m, 3H, CHOH, CH₂−N), 3.13−2.88 (m, 8H, N−CH₂), 2.25−2.09 (d, 2H, CH₂−N_ring). ¹³C NMR (75.5 MHz, D₂O) δ (ppm): 169.3, 148.9, 130.9, 58.8, 50.1, 48.0, 42.7, 40.1. FT-IR (ν, KBr): 3420, 3080, 1629, 1491, 1440 cm⁻¹.

The IL-HPA hybrid catalysts were prepared from the reaction between [TAHpy]Cl and phosphotungstate (Na₃PW₁₂O₄₀) in aqueous solution with different amounts of organic base (DETA) at room temperature for 24 h. The starting molar ratio of the reactants was DETA:[TAHpy]Cl:Na₃PW₁₂O₄₀ = x:1:1/3 (x stands for the molar ratio of DETA with [TAHpy]Cl). The obtained materials were named as [TAHpy]₃PW-x, x = 0, 1, and 2. [TAHpy]₃PW-0 was prepared in the absence of organic base (Yield: 40%). FT-IR (ν, KBr): 3429, 3093, 1620, 1458, 1380, 1070, 939, 845, 812 cm⁻¹. [TAHpy]₃PW-1: (Yield: 55%), FT-IR (ν, KBr): 3423, 3100, 1620, 1506, 1456, 1075, 942, 845, 805 cm⁻¹. [TAHpy]₃PW-2: (Yield: 58%), FT-IR (ν, KBr): 3427, 3108, 1622, 1502, 1450, 1070, 940, 851, 810 cm⁻¹.

Scheme S1 of the Supporting Information shows the synthetic routes of various control catalysts. 1-(2-Aminoethyl)pyridinium bromide ([AMpy]Br) was synthesized according to the literature.[24] For [AMpy]₃PW-0 (Yield: 94%), elemental analysis calcd (wt %): C 7.76, N 2.59, H 1.02, C/N = 3; found: C 7.65, N 2.55, H 1.16, C/N = 3. For [AMpy]₃PW-2 (Yield: 72%), elemental analysis found: (wt %): C 7.96, N 4.79, H 1.72, C/N = 1.66. N-(2,3-Dihydroxypropyl)-pyridinium chloride ([DHpy]Cl) was synthesized according to the literature.[37] For [DHpy]₃PW-0 (Yield: 74%), elemental analysis calcd (wt %): C 8.62, N 1.26, H 1.08, C/N = 6.84; found: C 8.51, N 1.23, H 1.04, C/N = 6.88. For [DHpy]₃PW-2 (Yield: 65%), elemental analysis found (wt %): C 8.82, N 2.63, H 1.54, C/N = 3.35. N-(3-aminoethoxyl-2- hydroxypropyl)pyridinium chloride ([AHpy]Cl) was prepared by ring-opening of [GIpy]Cl and ammonia−water.[36] For [AHpy]₃PW-0 (Yield: 35%), elemental analysis calcd (wt %): C 8.63, N 2.52, H 1.08, C/N = 3.42; found: C 8.78, N 2.54, H 1.12, C/N = 3.45. For [AHpy]₃PW-2 (Yield: 58%), elemental analysis found (wt %): C 10.93, N 4.5, H 2.02, C/N = 2.4.

DETA-PW was prepared by reaction of DETA (0.2 g, 1.9 mmol) with Na₃PW₁₂O₄₀ (1.85 g, 0.63 mmol) in aqueous solution to give a white solid. For DETA-PW, elemental analysis found (wt %): C 5.49, N 4.72, H 2.12, C/N = 1.16. DETA/[TAHpy]₃PW-0 was prepared by immersing [TAHpy]₃PW-0 in DETA aqueous solution with the molar ratio of DETA to [TAHpy]₃PW-0 as 3:1, following by stirring at room temperature for 24 h. Then the solid was centrifuged and dried. For

1919

dx.doi.org/10.1021/sc500259v | ACS Sustainable Chem. Eng. 2014, 2, 1918−1927

DETA/[TAHpy]$_3$PW-0, elemental analysis found (wt %): C 13.01 wt %, N 5.35 wt %, H 2.44 wt %, C/N = 2.43.

Catalytic Test. The hybrid catalysts were tested in the Knoevenagel condensation of benzaldehyde with ethyl cyanoacetate. A mixture of benzaldehyde (10 mmol), ethyl cyanoacetate (10 mmol), and the solvent (5 mL ethanol if necessary) were added to a 25 mL round-bottomed flask reactor equipped with a condenser under nitrogen atmosphere at the desired reaction temperature (70 °C). Calculated amount catalyst (0.1 g) was added into the reactor, and then the reaction slurry was stirred for 1 h under reflux. After reaction, the internal standard n-dodecane was added, and the resulting mixture was diluted with ethanol. The reaction mixture was centrifuged to remove the solid catalyst, and the liquid was analyzed by a gas chromatography (GC SP-6890) equipped with a FID detector and a capillary column (SE-54; 30 m × 0.32 mm × 0.25 μm). A three-run catalyst recycling was carried out for testing the reusability of catalyst. The catalyst was recovered from a reacted mixture by centrifugation, washed with hot ethanol three times, and dried in vacuum.

■ RESULTS AND DISCUSSION

Morphology and Pore Structure. The HPA-derived mesoporous solid base [TAHpy]$_3$PW-x can be prepared by the self-assembly of IL precursor [TAHpy]Cl with Na$_3$PW$_{12}$O$_{40}$ via controlling the amount of organic base DETA. Figure 1 and
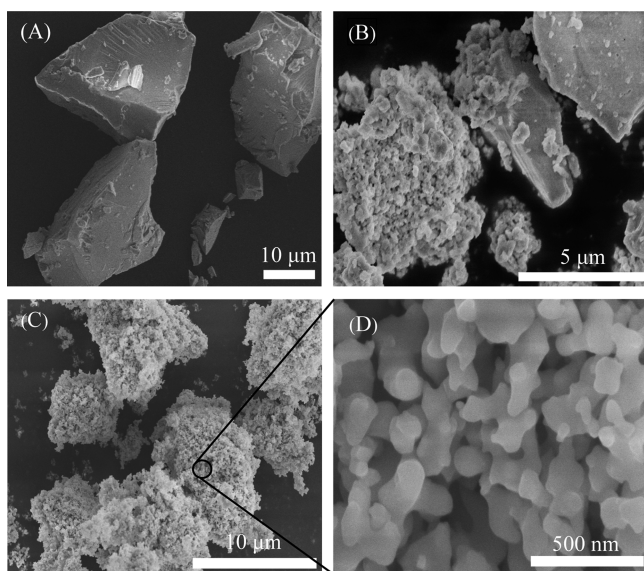
Figure 1. SEM images of [TAHpy]$_3$PW-x: (A) [TAHpy]$_3$PW-0, (B) [TAHpy]$_3$PW-1, and (C, D) [TAHpy]$_3$PW-2.

Figure S1 of the Supporting Information shows the optical photographs and SEM images of the obtained IL-HPA hybrids, the [TAHpy]$_3$PW-x (x = 0, 1, and 2) series. In the absence of DETA, the obtained [TAHpy]$_3$PW-0 sample is a hard black solid with a smooth surface (Figure S1,A, Supporting Information). The SEM image indicates that [TAHpy]$_3$PW-0 has a smooth prismatic block morphology with a length and width of several micrometers, and no substructure can be identified (Figure 1A), suggesting that [TAHpy]$_3$PW-0 has a dense structure. Very interestingly, when the organic base DETA (the molar ratio of DETA to [TAHpy]Cl is 1:1) was introduced in the synthesis system, a brown precipitate (the [TAHpy]$_3$PW-1 sample) forms. The optical photograph of [TAHpy]$_3$PW-1 shows that this sample is a mixture of a black and yellow solid (Figure S1,B, Supporting Information). SEM measurement shows the [TAHpy]$_3$PW-1 sample has a mixed

morphology of sponge-cake aggregation and smooth prismatic blocks (Figure 1B). The former is composed of relative uniform ellipsoidal particles with sizes of about 50 nm used to assemble a substructure at the micrometer level, and these aggregations are interwined with each other to form a nanoscale hollow structure. The later is similar to the particles of the [TAHpy]$_3$PW-0 sample. During synthesis, by increasing the amount of DETA to x = 2, the obtained [TAHpy]$_3$PW-2 sample changes to a loose yellow solid, which obtains a piece-like shape (Figure S1,C, Supporting Information). The SEM image (Figure 1C,D) shows that the primary particles of the [TAHpy]$_3$PW-2 sample are relatively uniform ellipsoidal particles with sizes of approximately 50 nm, and these particles are loosely packed to form sponge-cake aggregations with hollow structures that are similar to some particles for the [TAHpy]$_3$PW-1 sample. Throughout the whole sample of [TAHpy]$_3$PW-2, no intrinsic prismatic blocks are observed.

From the above results, it is found that the morphologies of [TAHpy]$_3$PW-1 and [TAHpy]$_3$PW-2 are different from that of [TAHpy]$_3$PW-0, and it is rational to suggest that the organic base DETA controls the self-assembly of cation and anion behavior, causing the morphology change from prismatic blocks with a size in micrometers to nanoscale spherical-like particles. These observations well demonstrate the above special morphological variation along with the self-assembly condition in the synthesis. In fact, combined with SEM and photographs of [TAHpy]$_3$PW-x, the sample [TAHpy]$_3$PW-1 can be considered as a transitional status between [TAHpy]$_3$PW-0 and [TAHpy]$_3$PW-2. In order to investigate the influence of the IL functional group on the morphology, various other IL-HPA counterparts are prepared from the self-assembly of Na$_3$PW$_{12}$O$_{40}$ and pyridinium IL-cations with varying amounts of hydroxyl or amino groups. For example, [AMpy]$_3$PW-0 prepared by using the monoamine-tethered cation shows rough spherical structures with sizes of about 2 μm (Figure 2A) . When the sample is prepared in the presence of a large amount of DETA, the obtained [AMpy]$_3$PW-2 material shows the morphology nanosheet with the size of 200−300 nm (Figure 2B). Moreover, the morphology is smooth angular blocks with sizes in micrometers by using the dihydroxyl-tethered cation to prepare the [DHpy]$_3$PW-0 hybrid (Figure 2C). But [DHpy]$_3$PW-2 also shows block-like morphology in micro-meter size even though the organic base DETA is added in the synthetic process (Figure 2D). The SEM image of [AHpy]$_3$PW-0 (Figure 2E) illustrates smooth blocks of several micrometers, while the similar primary particles and micro-morphology to [TAHpy]$_3$PW-2 are observed on the [AHpy]$_3$PW-2 sample (Figure 2F), which is also prepared by employing monoamine and monohydroxyl groups in the cation. These phenomena indicate that during the synthesis of the catalysts, the amine group and hydroxyl group in the IL-cation play key roles in the formation of the above special morphology. In the absence of the amino group, only large blocks are produced no mater of the presence of DETA, while different amounts of DETA will cause different morphologies if the pyridinium IL-cations contain at least one amino group.

The surface area and pore structure are characterized by the nitrogen sorption experiment. The sample [TAHpy]$_3$PW-0 is a nonporous material (Figure 3A, curve a) with a surface area of only 4.6 m^2 g^{-1} (Table 2), even lower than that of Na$_3$PW$_{12}$O$_{40}$. The nitrogen adsorption−desorption isotherm of [TAHpy]$_3$PW-1 is type IV with a H1-type hysteresis loop at a relatively higher partial pressure region of P/P_0 = 0.8−0.99
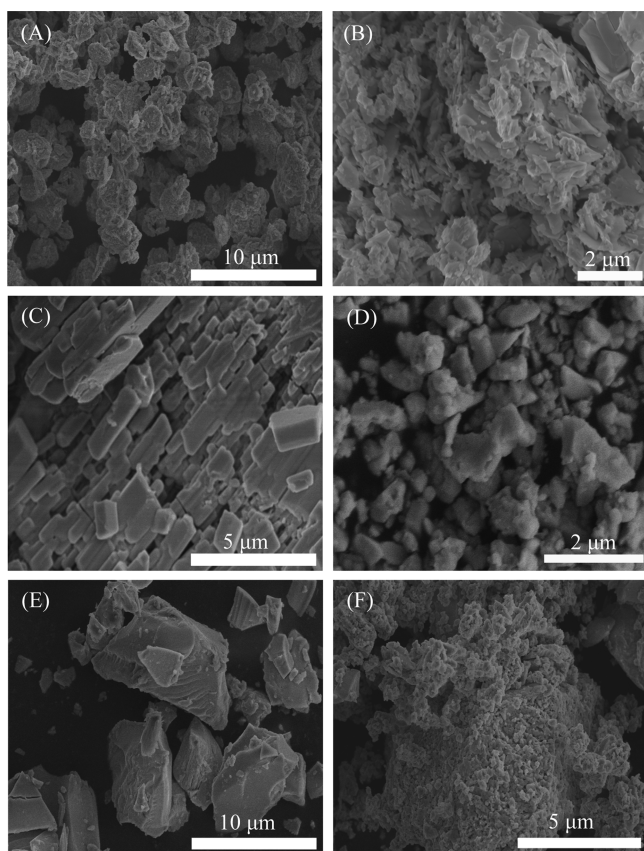
Figure 2. SEM images of (A) [AMpy]$_3$PW-0, (B) [AMpy]$_3$PW-2, (C) [DHpy]$_3$PW-0, (D) [DHpy]$_3$PW-2, (E) [AHpy]$_3$PW-0, and (F) [AHpy]$_3$PW-2.

(Figure 3A, curve b), reflecting the existence of mesopores. According to the Barrett–Joyner–Halenda model, the pore size of [TAHpy]$_3$PW-1 shows a wide window for distribution (Figure 3C, curve b). The sample [TAHpy]$_3$PW-1 has a moderate BET surface area of 23.2 m^2 g^{-1} and pore volume of 0.22 cm^3 g^{-1}. The nitrogen sorption isotherm of [TAHpy]$_3$PW-2 is type IV with a clear H1-type hysteresis loop at a relative low pressure of $P/P_0 = 0.7–0.9$ (Figure 3A, curve c), index of the typical mesoporous material. The sample [TAHpy]$_3$PW-2 exhibits a narrow pore size distribution with the most probable pore size of 9.2 nm (Figure 4C, curve c). The surface area and pore volume of [TAHpy]$_3$PW-2 is 26 m^2 g^{-1} and 0.09 cm^3 g^{-1}, respectively (Table 2). These values are consistent with the previously reported POM hybrid mesoporous materials with surface areas of 27–51 m^2 g^{-1}.[13,14,35] These results indicates that it can cause the formation of suitable mesostructures when the self-assembly of IL-cation and HPA occurs in the presence of a large amounts of DETA, and the organic base DETA amount significantly affects the self-assembly process. The other samples ([AMpy]$_3$PW-0, [AMpy]$_3$PW-2, [DHpy]$_3$PW-0, and [DHpy]$_3$PW-2) prepared from monoamine-tethered or dihydroxyl-tethered IL-cation all exhibit small surface areas, even in the existence of large amounts organic base DETA (Table 2). Therefore, amine and hydroxyl groups in the IL-cation jointly influence the formation of the porous structure. In order to support the above deduction, the [AHpy]$_3$PW-x series obtained from the IL-cation containing monoamine and monohydroxyl is characterized by the nitrogen sorption experiment. An obvious capillary condensation step at relative pressure of $P/P_0 = 0.7–0.9$ is observed for [AHpy]$_3$PW-2 (Figure 3B, curve e). The [AHpy]$_3$PW-2 has a moderate BET surface area of 11 m^2 g^{-1}, higher than those samples prepared
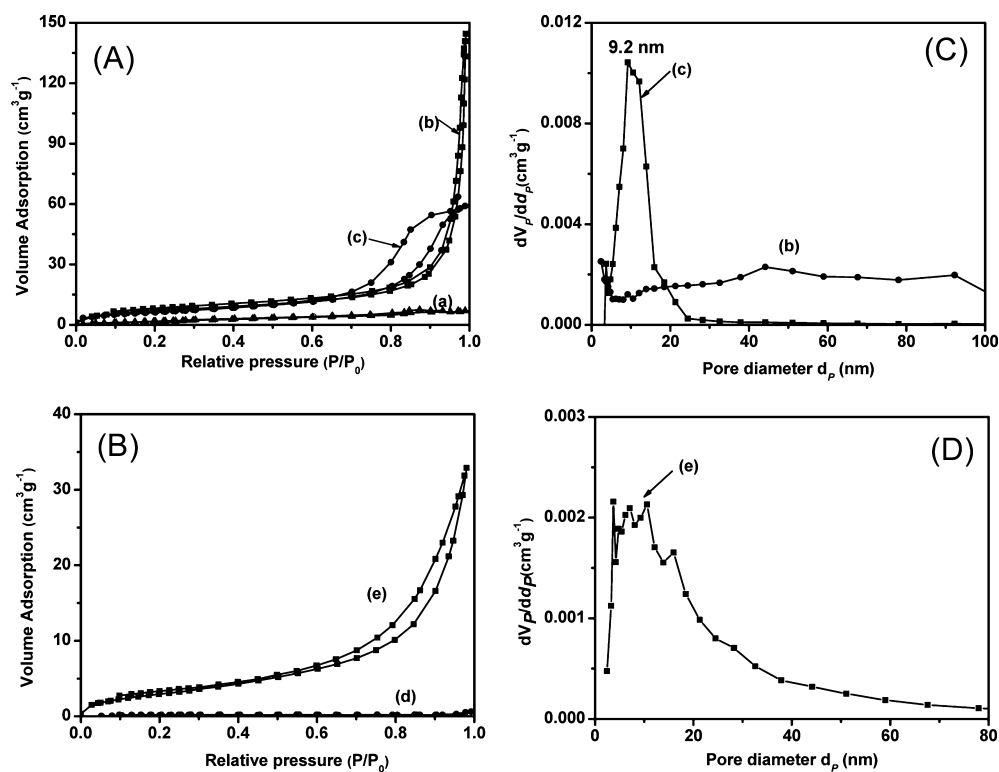
Figure 3. (A, B) N$_2$ sorption isotherms and (C, D) pore size distribution of (a) [TAHpy]$_3$PW-0, (b) [TAHpy]$_3$PW-1, (c) [TAHpy]$_3$PW-2, (d) [AHpy]$_3$PW-0, and (e) [AHpy]$_3$PW-2.
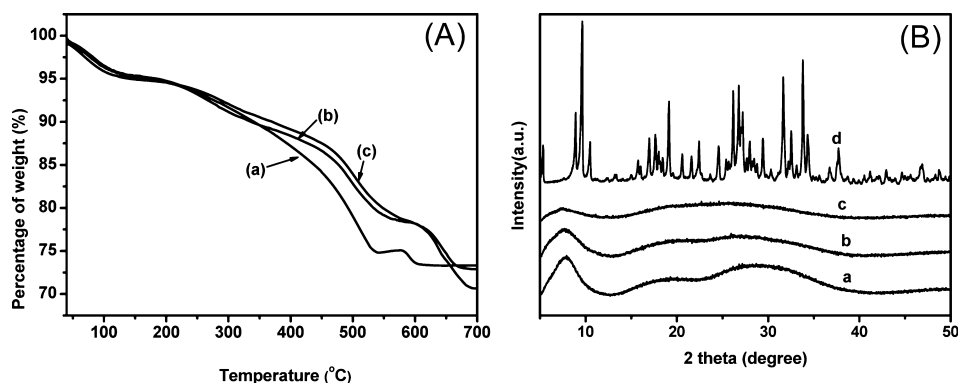
Figure 4. (A) TG curves and (B) XRD patterns of (a) [TAHpy]$_3$PW-0, (b) [TAHpy]$_3$PW-1, (c) [TAHpy]$_3$PW-2, and (d) Na$_3$PW$_{12}$O$_{40}$.

from the monoamine-tethered or dihydroxyl-tethered IL-cation but lower than [TAHpy]$_3$PW-2. These results indicate that the coexistence of large amounts of hydroxyl and amino groups in [TAHpy]Cl is important for the formation of a large surface area.

Chemical and Crystal Properties. The [TAHpy]$_3$PW-x series is further characterized by elemental analysis, TG, XRD, and FT-IR. For [TAHpy]$_3$PW-0, the elemental analysis found: C 12.01 wt %, N 4.60 wt %, H 2.07 wt %, C/N = 2.67 (Table 1), which are close to calcd: C 12.12 wt %, N 4.71 wt %, H 1.94

Table 1. Elemental Analysis of IL-HPA Hybrids [TAHpy]$_3$PW-x

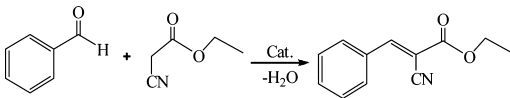| sample	C%	N%	H%	C/N	total weight loss %[a]
[TAHpy]$_3$PW-0	12.01	4.60	2.07	2.67	20.1
[TAHpy]$_3$PW-1	12.26	4.90	2.48	2.50	21.2
[TAHpy]$_3$PW-2	12.87	5.24	2.51	2.45	23.1

[a]TG data in the range of 230−680 °C.

wt %, C/N = 2.57, demonstrating the formula [TAHpy]$_3$PW-0 composed of three [TAHpy]$^+$ cations and one HPA. The TG curve (Figure 4A, curve a) showed a thermal stable structure for [TAHpy]$_3$PW-0 up to 230 °C. The weight loss at the early heating stage around 230 °C is due to the release of moisture and constitutional water, and the drastic weight loss above 230 °C is because of the decomposition of the organic moiety followed with the complete collapse of the inorganic Keggin HPA structure to form P$_2$O$_5$ and WO$_3$.[38] The total weight loss of 20.1% in the range of 230−680 °C is close to the theoretical data of 19.3%, which again verifies the chemical composition of

[TAHpy]$_3$PW-0. The TG curves (Figure 4A, curves b,c) of [TAHpy]$_3$PW-1 and [TAHpy]$_3$PW-2 also show stable structure of these two samples. It is found that the content of organic moiety is slightly influenced by the amount of organic base DETA. For example, the content of nitrogen of [TAHpy]$_3$PW-2 is higher than [TAHpy]$_3$PW-0 (Table 1). Furthermore, the content of the organic moiety of the IL-HPA hybrid [TAHpy]$_3$PW-2 is 23.1% (Table 1), higher than that of [TAHpy]$_3$PW-1 (21.2%) and [TAHpy]$_3$PW-0 (20.1%). The increase in the organic content is not derived from the partial substitution of the Na$^+$ from Na$_3$PW$_{12}$O$_{40}$ because an apparent decrease in the C/N molar ratio is observed. In other words, the C/N molar ratio will keep constant in the case of incomplete ion exchange between the IL-cation and HPA. Consequently, it can be deduced that a small part of DETA remains in the hybrids [TAHpy]$_3$PW-1 and [TAHpy]$_3$PW-2 during the synthesis process. Figure 4B illustrates the XRD patterns of the [TAHpy]$_3$PW-x hybrids and pure Na$_3$PW$_{12}$O$_{40}$. Na$_3$PW$_{12}$O$_{40}$ presents a set of diffraction peaks for the typical crystal structure of the sodium HPA salt with the Keggin PW-anions. However, for [TAHpy]$_3$PW-0, these peaks disappear after combining with IL-cation [TAHpy]$^+$, indicating an amorphous phase. It is suggested that the substitution of Na$^+$ by the large [TAHpy]$^+$ IL-cation has resulted in losing the long-range crystal order of PW-anions. A new broad Bragg reflection is visible at 2θ = 7.8° with d spacing of 1.1 nm, in agreement with the size for the structural units of the previously reported IL-HPA hybrid.[39] This feature suggests that the primary structural units (cations and anions) are distributed homogeneously throughout the secondary structure of the IL-HPA material with the formation of uniform microsized gaps,
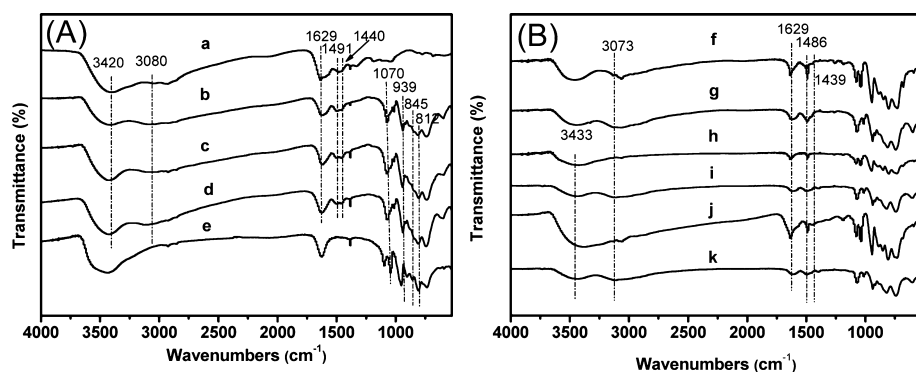
Figure 5. FT-IR spectra of (a) [TAHpy]Cl, (b) [TAHpy]$_3$PW-0, (c) [TAHpy]$_3$PW-1, (d) [TAHpy]$_3$PW-2, (e) Na$_3$PW$_{12}$O$_{40}$, (f) [AMpy]$_3$PW-0, (g) [AMpy]$_3$PW-2, (h) [DHpy]$_3$PW-0, (i) [DHpy]$_3$PW-2, (j) [AHpy]$_3$PW-0, and (k) [AHpy]$_3$PW-2.

Table 2. Textural Properties and Catalytic Performances of IL-HPA Catalysts in Solvent-Free Knoevenagel Condensation of Benzaldehyde with Ethyl Cyanoacetate[a]

entry	catalyst	S_{BET}[b] (m²/g)	V_p[c] (cm³/g)	D_{av}[d] (nm)	size of particle (μm)	character	conv.[e] (%)	sel.[f] (%)	TOF (h⁻¹)[g]
1	[TAHpy]₃PW-0	4.6	0.02	15.2	>5	black hard solid	7	100	8.3
2	[TAHpy]₃PW-1	23.2	0.22	33.8	0.05−10	black solid	88	100	104
3	[TAHpy]₃PW-2	26.0	0.09	15.7	0.05	brown solid	99	100	116
4[h]							97/94/94	100	−
5	DETA/[TAHpy]₃PW-0	−	−	−	>5	black hard solid	6	100	7.1
6	DETA-PW	3.2	0.01	14.8	>2	white solid	5	100	5.9
7	[AMpy]₃PW-0	6.2	0.05	29.6	>2	yellow solid	9	100	9.7
8	[AMpy]₃PW-2	7.1	0.05	33	0.2−0.3	yellow solid	89	100	96
9	[DHpy]₃PW-0	2.1	0.006	11.8	>5	white solid	5	100	5.5
10	[DHpy]₃PW-2	2.5	0.006	10.7	>2	white solid	4	100	4.4
11	[AHpy]₃PW-0	0.6	0.001	15.7	>5	black hard solid	6	100	6.6
12	[AHpy]₃PW-2	11.4	0.06	16.3	0.05	brown solid	85	100	93.6

[a]Reaction conditions: catalyst 0.1 g, benzaldehyde 10 mmol, ethyl cyanoacetate 10 mmol, 70 °C, 1 h. [b]BET surface area. [c]Total pore volume. [d]Average pore size. [e]GC conversion based on ethyl cyanoacetate. [f]GC selectivity for ethyl (E)-a-cyanocinnamate. [g]Turnover frequency: conversion of ethyl cyanoacetate (mmol)/(IL-cation in catalyst (mmol) × reaction time (h)). [h]Ethanol as solvent; reaction time 2 h.

which corresponds to the residual voids of ion-pair assembly.[40] As a result, the hybrid [TAHpy]₃PW-0 possesses a noncrystal structure but with certain regular ion-pair array. The hybrids [TAHpy]₃PW-1 and [TAHpy]₃PW-2 exhibit the same signal at the low angle of 7.8°, although with decreased intensities, implying a similar noncrystal structure. The sample DETA-PW is obtained via the reaction of DETA and Na₃PW₁₂O₄₀, and its XRD pattern presents many new characteristic peaks, reflecting the formation of new three-dimensional crystal structure (Figure S2, curve h, Supporting Information). However, the XRD patterns of [TAHpy]₃PW-1 and [TAHpy]₃PW-2 display amorphous phases and do not demonstrate any analogous characteristic peaks found in the XRD pattern of DETA-PW, suggesting that no DETA-PW phase forms with the existence of DETA in the synthetic system. The result suggests that organic base DETA does not react with Na₃PW₁₂O₄₀ during the preparation process of [TAHpy]₃PW-1 and [TAHpy]₃PW-2. It is clear that IL-HPA hybrids [TAHpy]₃PW-x have the same phase structures. In addition, UV−vis spectra indicate all the [TAHpy]₃PW-x samples have almost same electronic behavior (Figure S3, Supporting Information).

Figure 5 shows the FT-IR spectra of the selected samples to track the chemical functionalization. For [TAHpy]₃PW-0, the asymmetry broad band at 3093 cm⁻¹, attributed to the stretching vibration of N−H, 3429 cm⁻¹ to −OH, and 1458 cm⁻¹ to the stretching vibration of C−N, are similar to the observations at 3080, 3420, and 1440 cm⁻¹ for the IL precursor [TAHpy]Cl.[41] Further, the stretching vibration of the featured bands in pyridine are detected at 1620 and 1507 cm⁻¹ for [TAHpy]₃PW-0, similar to those peaks of [TAHpy]Cl at 1629 and 1491 cm⁻¹.[42] On the other hand, Na₃PW₁₂O₄₀ gives the four bands at 1098, 950, 858, and 808 cm⁻¹ featured for the Keggin structure of HPA, which are attributed to P−Oₐ (central oxygen), W = O (terminal oxygen), W−O_b−W (corner-sharing oxygen), and W−O_c−W (edge-sharing oxygen), respectively.[43] For [TAHpy]₃PW-0, the four Keggin bands are clearly detected, indicating that the framework structure of the PW-anion is well reserved. The shifts of the Keggin bands for [TAHpy]₃PW-0 imply the distortion of the Keggin POM

framework on account of the extension of the conjugated π electrons from organic cations to inorganic anions.[44,45] It is clear that the spectra of [TAHpy]₃PW-1 and [TAHpy]₃PW-2 are well consistent with [TAHpy]₃PW-0. But the band around 3108 cm⁻¹ that is assigned to the stretching vibration of N−H in [TAHpy]₃PW-1 and [TAHpy]₃PW-2 becomes stronger and broader than the corresponding band for [TAHpy]₃PW-0. A similar phenomenon can be observed in other control samples. For example, a narrow band at 3073 cm⁻¹ is detected for [AMpy]₃PW-0, which is in contrast to the broad band at 3084 cm⁻¹ for [AMpy]₃PW-2 (Figure 5, curves f,g).

Catalytic Evaluation in Knoevenagel Condensation. The basic catalytic performances of [TAHpy]₃PW-x hybrids are investigated in the solvent-free Knoevenagel reaction, which is a C=C bond formation reaction widely employed to synthesize the intermediates of fine chemicals.[46] First, the IL precursor and DETA are tested. The IL [GIpy]Cl offers a conversion of 37% and a selectivity of 100% in 30 min (Table S1, entry 1, Supporting Information). The ring-opening IL [TAHpy]Cl shows a conversion of 99% (Table S1, entry 2, Supporting Information) that is higher than the organic base DETA (91%, Table S1, entry 3, Supporting Information). The activity of the basic IL [TAHpy]Cl can be compared with the primary amine-functionalized IL,[47] tertiary amine-functionalized IL,[48,49] DABCO-base IL,[27] and even the Bronsted basic IL [bmIm]-OH.[50] Nevertheless, the critical problem associated with the use of ILs lies in the difficulty in catalyst separation as well as the recycling application because they are solvable in the reaction solution.[51] [TAHpy]₃PW-x materials are insoluble in most common solvents, including water, alcohols, ethyl acetate, acetic acid, acetonitrile, DMF, and DMSO, and thus can be used as the liquid−solid heterogeneous catalysts. Under the optimized reaction conditions, the catalytic activities of [TAHpy]₃PW-x are investigated in the solvent-free Knoevenagel condensation of benzaldehyde and ethyl cyanoacetate (Table 2). The nonporous catalyst [TAHpy]₃PW-0 with a particle size of >5 μm shows a conversion of 7% in 1 h (Table 2, entry 1). However, under the same reaction condition, the mesoporous IL-HPA hybrid [TAHpy]₃PW-1 with nanometer-

and micrometer-sized mixed particles offers a 88% conversion (entry 2). Very interestingly, the mesoporous IL-HPA hybrid [TAHpy]$_3$PW-2 with nanosized particles of about 50 nm exhibits a conversion of 99% and selectivity for ethyl (E)-α-cyanocinnamate of 100% (entry 3). In this case, the turnover frequency (TOF) for the catalyst is 116 h^{-1}, higher than [TAHpy]$_3$PW-0 (TOF = 8.3 h^{-1}) as well as [TAHpy]$_3$PW-2 (TOF = 104 h^{-1}) and dramatically even higher than the homogeneous IL precursor [TAHpy]Cl (TOF = 100 h^{-1}, Table S1, Supporting Information).

Moreover, the recycling catalytic performance of the solid base [TAHpy]$_3$PW-2 is investigated to measure the catalyst reusability. In the secondary run of solvent-free reaction, [TAHpy]$_3$PW-2 is thoroughly deactivated. The FT-IR spectrum for the recovered catalyst (Figure S5, curve c, Supporting Information) indicated that two extra bands are detected at 1724 and 1272 cm^{-1}, which are assigned to the C=O bond and C−O−C bond of ethyl cyanoacetate.[52] The result indicates that the recovered [TAHpy]$_3$PW-2 involves residues from the reaction mixture of high concentration that must have contaminated the basic sites, thereby resulting in a serious deactivation of the recovered catalyst in solvent-free reaction. Accordingly, the recycling experiment is performed in the Knoevenagel condensation with ethanol as the solvent for diluting concentration of the reactants for improving the catalyst reusability. Figure S6 of the Supporting Information depicts the influence of reaction time on the catalytic activity of [TAHpy]$_3$PW-2 under the above optimal conditions. High conversion of 97% is achieved with the optimal reaction time of 2 h. By facile centrifugation, [TAHpy]$_3$PW-2 is directly used in the next run. The used catalyst without any activation treatment is subjected to the same reaction, and it gives conversions of 97/94/94% for three runs (Table 2, entry 4). The result shows very slow decrease in activity in catalyst reuse, verifying that [TAHpy]$_3$PW-2 is a robust and reusable catalytic material for Knoevenagel condensation reaction. The IR spectrum for the thus recovered catalyst (Figure S5, curve b, Supporting Information) displays no extra band and is well consistent with that of the fresh one. The improvement of the reusability can be ascribed to the suitable solvent that provides the opportunity with timely leaching of adsorption of the residue on the catalyst surface. Considering the possible textural damage in a liquid-phase reaction, the textural parameters of the recovered [TAHpy]$_3$PW-2 are also tested. It is shown in Figure S7 of the Supporting Information that the morphology in the SEM image and the pore size distribution from the nitrogen adsorption−desorption isotherm for the recovered [TAHpy]$_3$PW-2 are similar to those for the fresh one (Figures 1 and 3). However, the sight decrease in BET surface areas from 26.0 to 18.5 m^2 g^{-1} may associate with the very slow decrease in activity in catalyst reuse.

Understanding of Catalytic Performance. Generally, the catalytic performance of a heterogeneous catalyst is not only determined by the active sites but also affected by the morphology and pore structure due to the mass transfer effect. The significant catalytic performance variation of [TAHpy]$_3$PW-x series cannot simply be assigned to the slight chemical discrepancy because they are prepared from the same IL and HPA salt precursor and should own more or less similar active sites. According to the elemental analysis and TG data of [TAHpy]$_3$PW-x, it is found that the content of nitrogen increases when x changes from 0 to 2 because a small amount organic base DETA is doped into the hybrids. So the serious

difference in the catalytic performance cannot exclude the responsibility of the doped organic base DETA. In order to investigate the potential catalytic role of doped organic base DETA, the sample DETA/[TAHpy]$_3$PW-0 is prepared by doping additional DETA on [TAHpy]$_3$PW-0 and assessed in the Knoevenagel condensation under the same condition. It only gives a conversion of 6% (Table 2, entry 5), indicating that the additionally doped DETA is incapable of remarkably activity. Furthermore, DETA-PW is prepared through doping DETA with Na$_3$PW$_{12}$O$_{40}$ and also exhibits a conversion of 5% in spite of high nitrogen content (Table 2, entry 6), suggesting that DETA directly doped on Na$_3$PW$_{12}$O$_{40}$ is inactive for the reaction. As mentioned above, the XRD patterns have excluded the existence of a significant amount DETA-PW phase in the [TAHpy]$_3$PW-1 or 2. Here, the catalytic performance further indicates that the possible catalytic function of the doped DETA is negligible for the reaction. In heterogeneous catalytic processes, it is known that the behavior of the activity is limited by the mass-transfer efficiency, thus the morphology and mesostructure play a key role in the reaction. The loosely packed nanoparticles with moderate mesopores favor fast mass transfer and the exposure of catalytically active sites on internal surfaces. Therefore, the catalytic activity of nonporous sample with nanosize morphology exhibits superior catalytic performance. The mesostructured IL-HPA hybrid [TAHpy]$_3$PW-1 displays a lower conversion than [TAHpy]$_3$PW-2 due to nanometer- and micrometer-sized mixed morphology. The reason that DETA-PW exhibits a low conversion can be also assigned to the bulky block morphology and nonporous structure (Figure S4, Supporting Information).

From the above analysis, the morphology and porous structure of [TAHpy]$_3$PW-x play an important role in the catalytic performance, and the small particle and mesoporous structure favor higher activity. To support such a proposal, various other IL-HPA hybrids such as [AMpy]$_3$PW-x, [DHpy]$_3$PW-x, and [AHpy]$_3$PW-x are tested in the same Knoevenagel reaction (Table 2). Unsurprisingly, the nonporous catalysts [AMpy]$_3$PW-0, [DHpy]$_3$PW-0, and [AHpy]$_3$PW-0 with block morphology all present low conversions of less than 10% (entries 7, 9, 11). Although hybrid [AMpy]$_3$PW-2 has a low surface area, the sample still offers a 89% conversion on account of its nanosheet morphology (entry 8), suggesting that the variation of the morphology is the major influential factor on the activity. The added organic base DETA does not change the block morphology for [DHpy]$_3$PW-2, so it shows a low conversion (entry 10). The hybrid [AHpy]$_3$PW-2 with comparably moderate surface area and nanosized particles offers a 85% conversion (entry 12), which is lower than that of [TAHpy]$_3$PW-2. The reason may be because [TAHpy]$_3$PW-2 has superior surface area and stronger basicity ascribed from the multiamine group in the IL precursor. These results further validate that the small particles and mesostructure favor better catalytic performance.

It has been speculated that the polarity of a solvent will significantly affect the reaction rate of Knoevenagel condensation, and a polar protic solvent such as ethanol is able to help the activation of the carbonyl substrate.[53] Generally, hybrid organic−inorganic solid base catalysts especially those containing a Lewis base are scarcely used for the reaction in the absence of polar protic solvent due to poor catalytic activity.[54−56] In this catalyst system, the mesoporous solid base [TAHpy]$_3$PW-2 shows excellent catalytic performance in the solvent-free Knoevenagel reaction. It is conjectured that the

Scheme 2. Proposed Catalytic Mechanism for [TAHpy]₃PW-2 Catalyzed Solvent-Free Knoevenagel Reaction
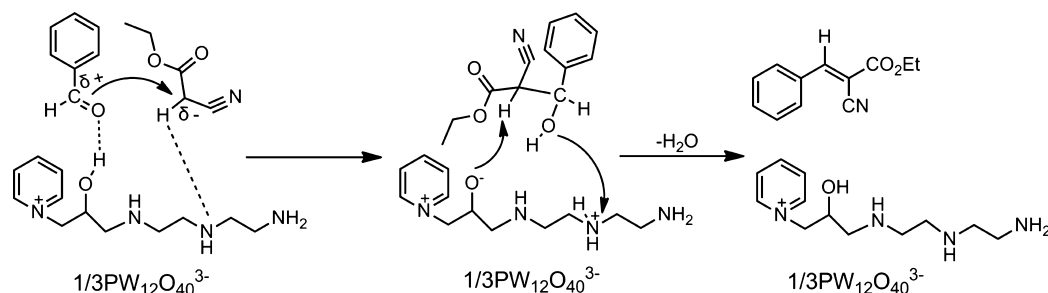
surface hydroxyl group can be instead of protic solvent to activate the carbonyl substrate.[57,58] For example, an acid–base bifunctional ionic solid catalyst [PySaIm]₃PW using a Schiff base structure was developed for solvent-free Knoevenagel condensations, in which the salicyl hydroxyl was able to form a hydrogen bond with aromatic aldehyde to function as a polar protic solvent.[58] Consequently, a catalytic mechanism is proposed for [TAHpy]₃PW-2-catalyzed solvent-free Knoevenagel condensation (Scheme 2). The hydroxyl group interacts with the oxygen of the carbonyl group in benzaldehyde by a hydrogen bond, through which the C=O bond is polarized. Meanwhile, as a Lewis basic site, the electron pair-bearing nitrogen of the amine group attacks the electron-deficient methylene hydrogen, forming an anionic methylene compound. The structure provides a suitable position for the bifunctional site with a comfortable distance, thereby allowing for a succeeding prompt reaction of the anionic methylene with the positive-charged carbon of the carbonyl into the C–C bonded intermediate that links the two reactants. Finally, the product is obtained by an immediate elimination of a water molecule from the intermediate, and meanwhile, [TAHpy]₃PW-2 is regenerated for the next catalytic cycle.

CONCLUSIONS

In summary, heteropolyanion-derived mesoporous solid base catalysts are prepared through specifically designing the IL-cation [TAHpy]⁺ to ionically assembly with the Keggin-structured heteroployanion $PW_{12}O_{40}^{3-}$ in basic conditions. During the synthesis, additional organic base DETA is used to control the morphology and pore structure of the hybrid catalyst, and the hydroxyl group and multiamine group of the IL precursor also favor the formation of small particles and mesopores. Owning to the special morphology and suitable mesostructure, the obtained hybrid displays good catalytic performance in Knoevenagel condensation of benzaldehyde with ethyl cyanoacetate, thus providing a new kind mesoporos solid base. Besides, the synthetic strategy of this study also provides some clues toward the design of morphology-controlled IL-HPA hybrids through controlling the external environment and countercation.

ASSOCIATED CONTENT

ⓢ Supporting Information

Synthetic route and XRD patterns of various counterpart catalysts, UV–vis spectra of [TAHpy]₃PW-x, solvent-free Knoevenagel condensation over IL precursor, influence of reaction time on Knoevenagel condensation with ethanol as the solvent over the catalyst [TAHpy]₃PW-2, FT-IR spectrum, and textural parameters of three times reused [TAHpy]₃PW-2. This material is available free of charge via the Internet at http://pubs.acs.org.

AUTHOR INFORMATION

Corresponding Author

*Tel.: +86-25-83172264. Fax: +86-25-83172261. E-mail: junwang@njtech.edu.cn.

Notes

The authors declare no competing financial interest.

REFERENCES

(1) Barbaro, P.; Liguori, F. Ion exchange resins: Catalyst recovery and recycle. *Chem. Rev.* **2009**, *109*, 515−529.

(2) Horváth, I. T.; Anastas, P. T. Innovations and green chemistry. *Chem. Rev.* **2007**, *107*, 2169−2173.

(3) Sheldon, R. A. Green and sustainable chemistry: Challenges and perspectives. *Green Chem.* **2008**, *10*, 359−360.

(4) Cole-Hamilton, D. J. Homogeneous catalysis − New approaches to catalyst separation, recovery, and recycling. *Science* **2008**, *299*, 1702−1706.

(5) Zhu, K.; Wang, D.; Liu, J. Self-assembled materials for catalysis. *Nano Res.* **2009**, *2*, 1−29.

(6) Bouhrara, M.; Ranga, C.; Fihri, A.; Shaikh, R. R.; Sarawade, P.; Emwas, A.-H.; Hedhili, M. N.; Polshettiwar, V. Nitridated fibrous silica (KCC-1) as a sustainable solid base nanocatalyst. *ACS Sustainable Chem. Eng.* **2013**, *1*, 1192−1199.

(7) Genna, D. T.; Wong-Foy, A. G.; Matzger, A. J.; Sanford, M. S. Heterogenization of homogeneous catalysts in metal-organic frameworks via cation exchange. *J. Am. Chem. Soc.* **2013**, *135*, 10586−10589.

(8) Hill, C. L. Introduction: Polyoxometalates-multicomponent molecular vehicles to probe fundamental issues and practical problems. *Chem. Rev.* **1998**, *98*, 1−2.

(9) Nisar, A.; Zhuang, J.; Wang, X. Construction of amphiphilic polyoxometalate mesostructures as a highly efficient desulfurization Catalyst. *Adv. Mater.* **2011**, *23*, 1130−1135.

(10) Nisar, A.; Wang, X. Surfactant-encapsulated polyoxometalate building blocks: Controlled assembly and their catalytic properties. *Dalton Trans.* **2012**, *41*, 9832−9845.

(11) Yang, Y.; Yue, L.; Li, H.; Maher, E.; Li, Y.; Wang, Y.; Wu, L.; Yam, V. W.-W. Photo-responsive self-assembly of an azobenzene-ended surfactant-encapsulated polyoxometalate complex for modulating catalytic reactions. *Small* **2012**, *8*, 3105−3110.

(12) Mizuno, N.; Kamata, K.; Nojima, S.; Yonehara, K. Flexible nonporous heterogeneous catalyst for size-selective oxidation through a bottom-up approach. *Angew. Chem., Int. Ed.* **2010**, *49*, 9972−9976.

(13) Vasylyev, M. V.; Neumann, R. New heterogeneous polyoxometalate based mesoporous catalysts for hydrogen peroxide mediated oxidation reactions. *J. Am. Chem. Soc.* **2004**, *126*, 884−890.

(14) Doherty, S.; Knight, J. G.; Ellison, J. R.; Weekes, D.; Harrington, R. W.; Hardacre, C.; Manyarb, H. An efficient recyclable peroxometalate-based polymer-immobilised ionic liquid phase (PIILP) catalyst for hydrogen peroxide-mediated oxidation. *Green Chem.* **2012**, *14*, 925−929.

(15) Sugahara, K.; Kimura, T.; Kamata, K.; Yamaguchi, K.; Mizuno, N. A highly negatively charged γ-Keggin germanodecatungstate efficient fo Knoevenagel condensation. *Chem. Commun.* **2012**, *48*, 8422−8424.

(16) Kimura, T.; Kamata, K.; Mizuno, N. A bifunctional tungstate catalyst for chemical fixation of CO₂ at atmospheric pressure. *Angew. Chem., Int. Ed.* **2012**, *51*, 6700−6703.

(17) Itagaki, S.; Kamata, K.; Yamaguchi, K.; Mizuno, N. Rhodium acetate/base-catalyzed N-silylation of indole derivatives with hydrosilanes. *Chem. Commun.* **2012**, *48*, 9269−9271.

(18) Zhang, Y.; Shen, Y.; Yuan, J.; Han, D.; Wang, Z.; Zhang, Q.; Niu, L. Design and synthesis of multifunctional materials based on an ionic-liquid backbone. *Angew. Chem., Int. Ed.* **2006**, *45*, 5867−5870.

(19) Ettedgui, J.; Neumann, R. Phenanthroline decorated by a crown ether as a module for metallorganic-polyoxometalate hybrid catalysts: The Wacker type oxidation of alkenes with nitrous oxide as terminal oxidant. *J. Am. Chem. Soc.* **2009**, *131*, 4−5.

(20) Haimov, A.; Neumann, R. An example of lipophiloselectivity: The preferred oxidation, in water, of hydrophobic 2-alkanols catalyzed by a cross-linked polyethyleneimine-polyoxometalate catalyst assembly. *J. Am. Chem. Soc.* **2006**, *128*, 15697−15700.

(21) Welton, T. Room-temperature ionic liquids. Solvents for synthesis and catalysis. *Chem. Rev.* **1999**, *99*, 2071−2083.

(22) Zhang, Q.; Zhang, S.; Deng, Y. Recent advances in ionic liquid catalysis. *Green Chem.* **2011**, *13*, 2619−2637.

(23) Hallett, J. P.; Welton, T. Room-temperature ionic liquids: Solvents for synthesis and catalysis. *Chem. Rev.* **2011**, *111*, 3508−3576.

(24) Bates, E. D.; Mayton, R. D.; Ntai, I.; Davis, J. H. CO₂ capture by a task-specific ionic liquid. *J. Am. Chem. Soc.* **2002**, *124*, 926−927.

(25) MacFarlane, D. R.; Pringle, J. M.; Johansson, K. M.; Forsyth, S. A.; Forsyth, M. Lewis base ionic liquids. *Chem. Commun.* **2006**, 1905−1917.

(26) Ranu, B. C.; Banerjee, S. Ionic liquid as catalyst and reaction medium. The dramatic influence of a task-specific ionic liquid, [bmIm]OH, in Michael addition of active methylene compounds to conjugated ketones, carboxylic esters, and nitriles. *Org. Lett.* **2005**, *7*, 3049−3052.

(27) Xu, D.-Z.; Liu, Y.; Shi, S.; Wang, Y. A simple, efficient and green procedure for Knoevenagel condensation catalyzed by [C₄dabco]-[BF₄] ionic liquid in water. *Green Chem.* **2010**, *12*, 514−517.

(28) Bourlinos, A. B.; Raman, K.; Herrera, R.; Zhang, Q.; Archer, L. A.; Giannelis, E. P. A liquid derivative of 12-tungstophosphoric acid with unusually high conductivity. *J. Am. Chem. Soc.* **2004**, *126*, 15358−15359.

(29) Rickert, P. G.; Antonio, M. R.; Firestone, M. A.; Kubatko, K.-A.; Szreder, T.; Wishart, J. F.; Dietz, M. L. Tetraalkylphosphonium polyoxometalate ionic liquids: Novel, organic-inorganic hybrid materials. *J. Phys. Chem. B* **2007**, *111*, 4685−4692.

(30) Leng, Y.; Wang, J.; Zhu, D.; Ren, X.; Ge, H.; Shen, L. Heteropolyanion-based ionic liquids: reaction-induced self-separation catalysts for esterification. *Angew. Chem., Int. Ed.* **2009**, *48*, 168−171.

(31) Leng, Y.; Wang, J.; Zhu, D.; Wu, Y.; Zhao, P. Sulfonated organic heteropolyacid salts: Recyclable green solid catalysts for esterifications. *J. Mol. Catal.* **2009**, *313*, 1−6.

(32) Zhang, W.; Leng, Y.; Zhao, P.; Wang, J.; Zhu, D.; Huang, J. Heteropolyacid salts of N-methyl-2-pyrrolidonium as highly efficient and reusable catalysts for Prins reactions of styrenes with formalin. *Green Chem.* **2011**, *13*, 832−834.

(33) Leng, Y.; Wang, J.; Zhu, D.; Zhang, M.; Zhao, P.; Long, Z.; Huang, J. Polyoxometalate-based amino-functionalized ionic solid catalysts lead to highly efficient heterogeneous epoxidation of alkenes with H₂O₂. *Green Chem.* **2011**, *13*, 1636−1639.

(34) Zhao, P.; Leng, Y.; Zhang, M.; Wang, J.; Wu, Y.; Huang, J. A polyoxometalate-based Pdᴵᴵ-coordinated ionic solid catalyst for

heterogeneous aerobic oxidation of benzene to biphenyl. *Chem. Commun.* **2012**, *48*, 5721−5723.

(35) Chen, G.; Zhou, Y.; Zhao, P.; Long, Z.; Wang, J. Mesostructured dihydroxy-functionalized guanidinium-based polyoxometalate with enhanced heterogeneous catalytic activity in epoxidation. *ChemPlusChem.* **2013**, *78*, 561−569.

(36) Demberelnyamba, D.; Yoon, S. J.; Lee, H. New epoxide molten salts: Key intermediates for designing novel ionic liquids. *Chem. Lett.* **2004**, *33*, 560−561.

(37) Khalahi-Nezhad, A.; Mohammadi, S. Highly efficient synthesis of novel Morita−Baylis−Hillman adducts from activated ketones using a DABCO-based hydroxy ionic liquid (HIL) as a recyclable catalyst-solvent. *Synthesis* **2012**, *44*, 1725−1735.

(38) Rao, G. R.; Rajkumar, T.; Varghese, B. Synthesis and characterization of 1-butyl 3-methyl imidazolium phosphomolybdate molecular salt. *Solid State Sci.* **2009**, *11*, 36−42.

(39) Yan, X.; Zhu, P.; Fei, J.; Li, J. Self-assembly of peptide-inorganic hybrid spheres for adaptive encapsulation of guests. *Adv. Mater.* **2010**, *22*, 1283−1287.

(40) Okuhara, T.; Nakato, T. Catalysis by porous heteropoly compounds. *Catal. Surv. Jpn.* **1998**, *2*, 31−44.

(41) Ribeiro, S. M.; Serra, A. C.; Rocha Gonsalves, A.M. d'A. Silica grafted polyethylenimine as heterogeneous catalyst for condensation reactions. *Appl. Catal., A* **2011**, *399*, 126−133.

(42) Vimont, A.; Travert, A.; Binet, C.; Pichon, C.; Mialane, P.; Sécheresse, F.; Lavalley, J.-C. Relationship between infrared spectra and stoichiometry of pyridine-H₃PW₁₂O₄₀ salts using a new TGA-infrared coupling. *J. Catal.* **2006**, *241*, 221−224.

(43) Rao, P. M.; Wolfson, A.; Kababya, S.; Vega, S.; Landau, M. V. Immobilization of molecular H₃PW₁₂O₄₀ heteropolyacid catalyst in alumina-grafted silica-gel and mesostructured SBA-15 silica matrices. *J. Catal.* **2005**, *232*, 210−215.

(44) Douvas, A. M.; Yannakopoulou, K.; Argitis, P. Thermally-induced acid generation from 18-molybdodiphosphate and 18-tungstodiphosphate within poly(2-hydroxyethyl methacrylate) films. *Chem. Mater.* **2010**, *22*, 2730−2740.

(45) Felices, L. S.; Vitoria, P.; Gutierrez-Zorrilla, J. M.; Reinoso, S.; Etxebarria, J.; Lezama, L. A novel hybrid inorganic-metalorganic compound based on a polymeric polyoxometalate and a copper complex: Synthesis, crystal structure and topological studies. *Chem.—Eur. J.* **2004**, *10*, 5138−5146.

(46) Corma, A.; Martín-Aranda, R. M.; Sánchez, F. Zeolites as base catalysts. Preparation of calcium antagonists intermediates by condensation of benzaldehyde with ethyl acetoacetate. *Stud. Surf. Sci. Catal.* **1991**, *59*, 503−511.

(47) Cai, Y.; Peng, Y.; Song, G. Amino-functionalized ionic liquid as an efficient and recyclable catalyst for Knoevenagel reactions in water. *Cata. Lett.* **2006**, *109*, 1−2.

(48) Luo, J.; Xin, T.; Wang, Y. A PEG bridged tertiary amine functionalized ionic liquid exhibiting thermoregulated reversible biphasic behavior with cyclohexane/isopropanol: synthesis and application in Knoevenagel condensation. *New J. Chem.* **2013**, *37*, 269−273.

(49) Forsyth, S. A.; Fröhlich, U.; Goodrich, P.; Gunaratne, H. Q. N.; Hardacre, C.; McKeown, A.; Seddon, K. R. Functionalised ionic liquids: Synthesis of ionic liquids with tethered basic groups and their use in Heck and Knoevenagel reactions. *New J. Chem.* **2010**, *34*, 723−731.

(50) Ranu, B. C.; Jana, R. Ionic liquid as catalyst and reaction medium-a simple, efficient and green procedure for Knoevenagel condensation of aliphatic and aromatic carbonyl compounds using a task-specific basic ionic liquid. *Eur. J. Org. Chem.* **2006**, 3767−3770.

(51) Valkenberg, M. H.; deCastro, C.; Hölderich, W. F. Immobilisation of ionic liquids on solid supports. *Green Chem.* **2002**, *4*, 88−93.

(52) Wirz, R.; Ferri, D.; Baiker, A. ATR-IR spectroscopy of pendant NH₂ groups on silica involved in the Knoevenagel condensation. *Langmuir* **2006**, *22*, 3698−3706.

(53) Rodriguez, I.; Sastre, G.; Corma, A.; Iborra, S. Catalytic activity of proton sponge: Application to Knoevenagel condensation reactions. *J. Cata.* **1999**, *183*, 14−23.

(54) Xing, R.; Wu, H.; Li, X.; Zhao, Z.; Liu, Y.; Chen, L.; Wu, P. Mesopolymer solid base catalysts with variable basicity: preparation and catalytic properties. *J. Mater. Chem.* **2009**, *19*, 4004−4011.

(55) Zhang, Y.; Zhao, Y.; Xia, C. Basic ionic liquids supported on hydroxyapatite-encapsulated γ-Fe_2O_3 nanocrystallites: An efficient magnetic and recyclable heterogeneous catalyst for aqueous Knoevenagel condensation. *J. Mol. Catal.* **2009**, *306*, 107−112.

(56) Gianotti, E.; Diaz, U.; Colucciab, S.; Corma, A. Hybrid organic-inorganic catalytic mesoporous materials with proton sponges as building blocks. *Phys. Chem. Chem. Phys.* **2011**, *13*, 11702−11709.

(57) Han, J.; Xu, Y.; Su, Y.; She, X.; Pan, X. Guanidine-catalyzed Henry reaction and Knoevenagel condensation. *Catal. Commun.* **2008**, *9*, 2077−2079.

(58) Zhang, M.; Zhao, P.; Leng, Y.; Chen, G.; Wang, J.; Huang, J. Schiff base structured acid-base cooperative dual sites in an ionic solid catalyst lead to efficient heterogeneous Knoevenagel condensations. *Chem.—Eur. J.* **2012**, *18*, 12773−12782.